2013

Sensorless Control of Surface-Mounted Permanent-Magnet Synchronous Machines for Low-Speed Operation Based on High-Frequency Square-Wave Voltage Injection

Yue Zhao
University of Nebraska-Lincoln, yue.zhao@huskers.unl.edu

Zhe Zhang
University of Nebraska-Lincoln

Cong Ma
University of Nebraska-Lincoln

Wei Qiao
University of Nebraska-Lincoln, wqiao@engr.unl.edu

Liyan Qu
University of Nebraska-Lincoln, lqu2@unl.edu

Sensorless Control of Surface-Mounted Permanent-Magnet Synchronous Machines for Low-Speed Operation Based on High-Frequency Square-Wave Voltage Injection

Yue Zhao, Zhe Zhang, and Cong Ma
Student Member, IEEE
Power and Energy Systems Laboratory
Department of Electrical Engineering
University of Nebraska-Lincoln
Lincoln, NE 68588-0511 USA
yue.zhao@huskers.unl.edu

[1]Wei Qiao and [2]Liyan Qu
[1]Senior Member, IEEE; [2]Member, IEEE
Power and Energy Systems Laboratory
Department of Electrical Engineering
University of Nebraska-Lincoln
Lincoln, NE 68588-0511 USA
wqiao@engr.unl.edu; liyanqu@ieee.org

Abstract—This paper proposes a high-frequency signal injection-based position estimation scheme for surface-mounted permanent-magnet synchronous machines (SPMSM) operating in the low-speed range. A square-wave voltage vector is injected in the estimated rotating reference frame. The rotor position information is then extracted from the envelopes of the resulting induced high-frequency currents in the stationary reference frame. The proposed position estimation method has almost no dependence on machine asymmetric properties and, therefore, is well suited for SPMSM applications. Simulation results are provided to verify the effectiveness of the proposed method from 1 Hz to 50 Hz electric fundamental frequency under all load conditions. Experimental results on a 2.4-kW SPMSM in both sensorless speed and torque controls are also provided to validate the proposed method. The sensorless speed control can be achieved as low as 0.3 Hz electric fundamental frequency.

Index Terms—Position estimation, sensorless control, signal injection, square wave, surface-mounted permanent-magnet synchronous machine (SPMSM).

I. INTRODUCTION

Electromechanical sensors are commonly used to obtain the accurate rotor position information for high-performance permanent-magnet synchronous machine (PMSM) drives. However, the use of these sensors not only increases the cost, size, weight, and wiring complexity, but also reduces mechanical robustness of the drive systems. In the past decades, much research effort has gone into the development of sensorless drives that have comparable dynamic performance with respect to the sensor-based drives [1], [2].

In the literature, there are two major categories of methods for rotor position/speed observation for PMSMs. The first category of methods estimates the position related states, e.g., back electromagnetic force (EMF) [3], [4] and flux [5], in the PMSM fundamental frequency model. Based on these estimated system states, the rotor position information can be extracted [6]. However, this category of methods has poor performance or even fails in the low-speed region and at standstill due to low signal-to-noise ratio (SNR) of the system states. The other category of methods, which is particularly effective in the low-speed range, utilizes the anisotropic properties of the machine, e.g., rotor saliency and/or the saturation of the stator iron. By using a pulsating [7] or rotating [8] high-frequency signal injection (HFSI) method, position estimation can be performed. Both sinusoidal and square waves [9] are effective candidates for the injected carrier signals.

The conventional HFSI methods rely on a rotor position dependent spatial saliency. For an interior PMSM (IPMSM), a large spatial saliency, i.e., difference between d-axis and q-axis inductances, inherently exists. Thus, the HFSI methods are well suited for IPMSMs. For a surface-mounted PMSM (SPMSM), the spatial saliency can be related to the saturation effect of the stator leakage flux or main flux [10]. However, due to the symmetric rotor structure of the SPMSM, the dependence of the spatial inductance distribution on the rotor position is weak. This leads to a low SNR of the saliency related signals, e.g., the amplitudes of the induced high-frequency currents. Thus, when applying an HFSI method to an SPMSM, a narrow-bandwidth saliency tracking observer is required to extract the saliency related signal. However, the performance of the sensorless drive will degrade due to the narrow bandwidth design. To solve this problem and improve the position estimation performance, several adaptive or nonlinear observers have been proposed [11], [12]. In recent years, instead of tracking a low SNR spatial saliency signal, other physical attributes, e.g., high-frequency impedance [12], rotor and stator resistances [13], and eddy current losses [14], have been utilized for position estimation.

In this paper, a pulsating voltage vector is injected into an estimated γ-δ rotating reference frame. In the conventional methods [7], when a pulsating signal is injected into γ axis, a position related signal, i.e., the error between the estimated and actual positions, can be detected from the induced high-frequency current in the δ axis. The magnitude of the signal depends on machine asymmetry. Therefore, the conventional methods are not effective for SPMSMs. This paper proposes a method to extract the rotor position from the envelopes of the induced high-frequency current signals in the stationary reference frame. The proposed method has nearly zero dependence on machine asymmetry and, therefore, is well suited for SPMSMs, especially when the difference between the high-frequency impendences on different axes is negligible. Since only the envelopes of the high-frequency currents are used, the proposed method injects a square-wave

voltage signal, instead of a high-frequency sinusoidal voltage signal. This increases the upper bandwidth of the sensorless speed controller and will have a better potential for practical applications. Simulation and experimental results are provided to demonstrate the effectiveness of the proposed method for low-speed sensorless control of SPMSMs.

II. HIGH-FREQUENCY MODEL OF AN SPMSM

A. High-Frequency Impedance Model

The dynamics of an SPMSM can be expressed in a d-q rotating reference frame as:

$$\begin{bmatrix} v_d \\ v_q \end{bmatrix} = \begin{bmatrix} R_s + L_s p & -\omega_{re} L_s \\ \omega_{re} L_s & R_s + L_s p \end{bmatrix} \begin{bmatrix} i_d \\ i_q \end{bmatrix} + \begin{bmatrix} 0 \\ \omega_{re} \lambda_m \end{bmatrix} \qquad (1)$$

where p is the derivative operator; v_d and v_q are the stator voltages; i_d and i_q are the stator currents; ω_{re} is the rotor electrical angular rotating speed in rad/s; L_s is the stator inductance; and R_s is the stator resistance. If high-frequency pulsating voltage signals, $v_{d,h}$ and $v_{q,h}$, whose frequency is sufficiently higher than the rotor speed, are injected into the machine stator windings, high-frequency currents, $i_{d,h}$ and $i_{q,h}$, will be generated. To reduce extra losses and minimize the effect on the normal operation of the drive system, the magnitudes of the injected voltage signals are usually small, so as the induced currents. However, due to their high frequency, the derivatives of these signals can be quite large. Therefore, when considering the high-frequency components, the off-diagonal cross-coupling terms in (1) are sufficiently smaller than the diagonal terms and can be ignored. Similarly, in the low-speed region and at standstill, the back EMF term can also be neglected. Consequently, the high-frequency model of the SPMSM in the low-speed region can be expressed as:

$$\begin{bmatrix} v_{d,h} \\ v_{q,h} \end{bmatrix} = \begin{bmatrix} Z_{d,h} & 0 \\ 0 & Z_{q,h} \end{bmatrix} \begin{bmatrix} i_{d,h} \\ i_{q,h} \end{bmatrix} \qquad (2)$$

where $Z_{d,h} = R_{d,h} + j\omega_h \cdot L_{d,h}$ and $Z_{q,h} = R_{q,h} + j\omega_h \cdot L_{q,h}$ are the d-axis and q-axis high-frequency impedances, respectively; ω_h is frequency of the injected signals; $R_{d,h}$ and $R_{q,h}$ are the d-axis and q-axis high-frequency resistances, respectively; and $L_{d,h}$ and $L_{q,h}$ are the d-axis and q-axis high-frequency inductances, respectively.

B. Spatial Saliency Property of an SPMSM

Finite-element analysis (FEA) is performed to investigate the spatial saliency property of an SPMSM with high-frequency signals injected. The SPMSM has 6 poles, 18 slots and distributed windings. A 1-V, 400-Hz sinusoidal pulsating voltage vector is injected into the d axis. The distributions of the magnetic flux lines and flux density when the rotor positions are $0°$, $30°$, $60°$, and $90°$ are shown in Fig. 1.

The result of FEA shows that the rotor position has little effect on the spatial distribution of the high-frequency resistance. The spatial distribution of the high-frequency self-inductance, as show in Fig. 2, is more position dependent than that of the resistance, but is still insufficient for accurate position estimation. Increasing the magnitude and frequency (e.g., using 1 kHz or even a higher frequency) of the injected signals will increase the saliency ratio, which however also results in higher losses and increased harmonics in the terminal voltages of the inverter.

III. HIGH-FREQUENCY PULSATING SIGNAL INJECTION

In this section, the high-frequency impedance model (2) is used to derive the expression for the induced high-frequency currents for rotor position estimation. The pulsating voltage vector is injected into the estimated γ-δ rotating reference
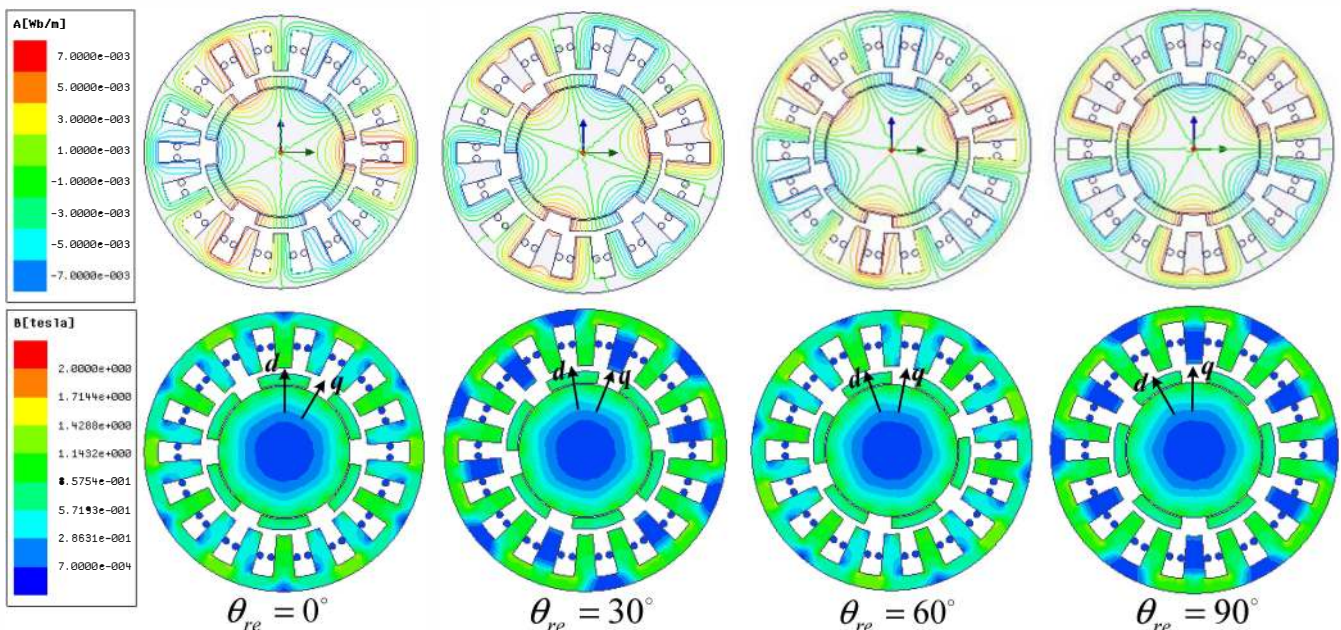

Fig. 1.   Distributions of flux lines and flux density of an SPMSM at different rotor positions.

frame. The angle between γ axis and α axis, which is aligned with the direction of the phase A magnetic axis, is defined as the estimated position, as shown in Fig. 3. The error between the actual and estimated positions is denoted as $\Delta\theta$. In this section, the conventional position estimation scheme using pulsating sinusoidal voltage injection is briefly presented. That method is highly dependent on rotor saliency and, thus, is not effective for SPMSMs. To solve this problem, a position estimation method independent on rotor spatial saliency is proposed. The proposed method is firstly discussed based on a sinusoidal voltage injection. A square-wave voltage injection scheme is then proposed to improve the upper bandwidth of the sensorless speed control.
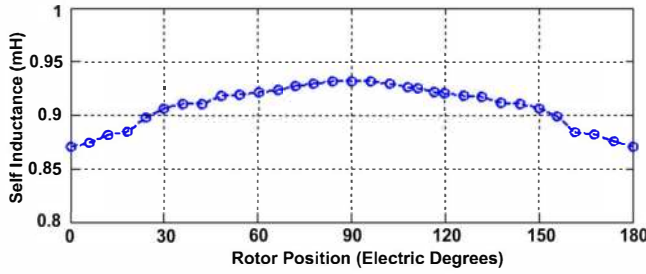

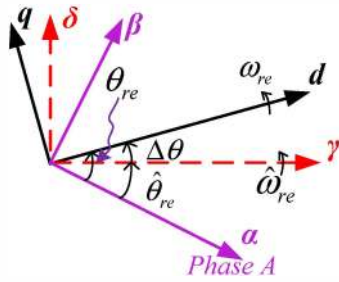Fig. 2.   Spatial distribution of high-freqeuncy self-inductance.

Fig. 3.   Relationships among the α-β stationary reference frame, the ideal d-q rotating reference frame, and the estimated γ-δ rotating reference frame.

A.   Sinusoidal Signal Injection

A sinusoidal pulsating voltage vector described by (3) is injected into the estimated γ-δ rotating reference frame.

$$v_{\gamma\delta,h} = \begin{bmatrix} v_{\gamma,h} \\ v_{\delta,h} \end{bmatrix} = V_h \begin{bmatrix} \cos(\omega_h t) \\ 0 \end{bmatrix} \tag{3}$$

where ω_h and V_h are the frequency and amplitude of the injected voltage vector. Projecting $v_{\gamma\delta,h}$ on the d- and q- axes, the resulting voltage vector, $v_{dq,h}$, can be expressed as:

$$v_{dq,h} = \begin{bmatrix} v_{d,h} \\ v_{q,h} \end{bmatrix} = \begin{bmatrix} \cos(\Delta\theta) & \sin(\Delta\theta) \\ -\sin(\Delta\theta) & \cos(\Delta\theta) \end{bmatrix} \begin{bmatrix} v_{\gamma,h} \\ v_{\delta,h} \end{bmatrix} = v_{\gamma,h} \begin{bmatrix} \cos(\Delta\theta) \\ -\sin(\Delta\theta) \end{bmatrix} \tag{4}$$

According to (2) and (4), the induced high-frequency currents in the ideal d-q reference frame can be determined.

$$\begin{bmatrix} i_{d,h} \\ i_{q,h} \end{bmatrix} = v_{\gamma,h} \begin{bmatrix} \cos(\Delta\theta)/Z_{d,h} \\ -\sin(\Delta\theta)/Z_{q,h} \end{bmatrix} \tag{5}$$

In the conventional method, the position information is extracted from the induced current signal in the estimated rotating reference frame as follows:

$$\begin{bmatrix} i_{\gamma,h} \\ i_{\delta,h} \end{bmatrix} = \begin{bmatrix} \cos(\Delta\theta) & -\sin(\Delta\theta) \\ \sin(\Delta\theta) & \cos(\Delta\theta) \end{bmatrix} \begin{bmatrix} i_{d,h} \\ i_{q,h} \end{bmatrix} = v_{\gamma,h} \begin{bmatrix} \dfrac{\cos^2(\Delta\theta)}{Z_{d,h}} + \dfrac{\sin^2(\Delta\theta)}{Z_{q,h}} \\ \dfrac{(Z_{q,h} - Z_{d,h})}{2 Z_{d,h} Z_{q,h}} \sin(2\Delta\theta) \end{bmatrix} \tag{6}$$

As shown in (6), the position tracking error, $\Delta\theta$, is contained in $i_{\delta,h}$. However, the magnitude of $i_{\delta,h}$ depends on the rotor saliency. If the saliency is small, as in an SPMSM where $(Z_{q,h} - Z_{d,h}) \ll (Z_{q,h} + Z_{d,h})$, (6) will not be effective for position estimation due to the low SNR of the saliency related signal. To solve this problem, a better position observation method which has low dependence on the rotor saliency is needed for SPMSMs in the low-speed region.

In the proposed method, the rotor position is obtained from the induced current vector, $i_{\alpha\beta,h}$, in the α-β reference frame as follows:

$$i_{\alpha\beta,h} = \begin{bmatrix} i_{\alpha,h} \\ i_{\beta,h} \end{bmatrix} = \begin{bmatrix} \cos(\theta_{re}) & -\sin(\theta_{re}) \\ \sin(\theta_{re}) & \cos(\theta_{re}) \end{bmatrix} \begin{bmatrix} i_{d,h} \\ i_{q,h} \end{bmatrix}$$
$$= V_h \cos(\omega_h t) \begin{bmatrix} \dfrac{\cos(\Delta\theta)}{Z_{d,h}} \cos(\theta_{re}) + \dfrac{\sin(\Delta\theta)}{Z_{q,h}} \sin(\theta_{re}) \\ \dfrac{\cos(\Delta\theta)}{Z_{d,h}} \sin(\theta_{re}) - \dfrac{\sin(\Delta\theta)}{Z_{q,h}} \cos(\theta_{re}) \end{bmatrix} \tag{7}$$

If the position error, $\Delta\theta$, is small enough such that $\sin(\Delta\theta) \approx 0$ and $\cos(\Delta\theta) \approx 1$, then (7) can be simplified as:

$$\begin{bmatrix} i_{\alpha,h} \\ i_{\beta,h} \end{bmatrix} \approx \frac{V_h \cos(\omega_h t)}{Z_{d,h}} \begin{bmatrix} \cos(\theta_{re}) \\ \sin(\theta_{re}) \end{bmatrix} \tag{8}$$

As shown in (8), if the rotating frequency of the machine is much smaller than the frequency of the injected signal, the envelopes of $i_{\alpha\beta,h}$ are position dependent signals. If the envelopes are extracted, the rotor position can be obtained.

Since for an SPMSM the difference between $Z_{d,h}$ and $Z_{q,h}$ can be neglected (i.e., $Z_{d,h} \approx Z_{q,h} \approx Z_{s,h}$), (7) can be simplified as follows:

$$\begin{bmatrix} i_{\alpha,h} \\ i_{\beta,h} \end{bmatrix} = \frac{V_h \cos(\omega_h t)}{Z_{s,h}} \begin{bmatrix} \cos(\theta_{re} - \Delta\theta) \\ \sin(\theta_{re} - \Delta\theta) \end{bmatrix} = \frac{V_h \cos(\omega_h t)}{Z_{s,h}} \begin{bmatrix} \cos(\hat\theta_{re}) \\ \sin(\hat\theta_{re}) \end{bmatrix} \tag{9}$$

Equations (8) and (9) are both simplified versions of (7). Although they are derived based on different assumptions, both of them indicate that the rotor position information can be directly obtained from the envelopes of $i_{\alpha\beta,h}$, if a high-frequency pulsating voltage vector is injected in the γ-δ reference frame.

In practical applications, the conventional HFSI method, which injects a sinusoidal voltage signal, often suffers from the problem of a narrow bandwidth, due to the limited PWM frequency. Fig. 4(a) illustrates the relationship between an injected sinusoidal signal and a PWM carrier waveform. Assume that at standstill and in the low-speed region, the PWM switching frequency and sampling frequency are 2.5 kHz. As shown in Fig. 4(a), the frequency of the injected

signal is 500 Hz, such that there are only 5 samples in one period of the injected sinusoidal signal. Thus, the resulting discrete-time waveform (i.e., the dash-line waveform) is far away from a sinusoidal signal. This will become worse if the frequency of the injected signal further increases. As a consequence, the analysis presented early in this section will no longer be valid. Therefore, the highest frequency of the injected sinusoidal signal is limited by the PWM switching frequency, which further limits the upper bandwidth of the sensorless speed controller [9].
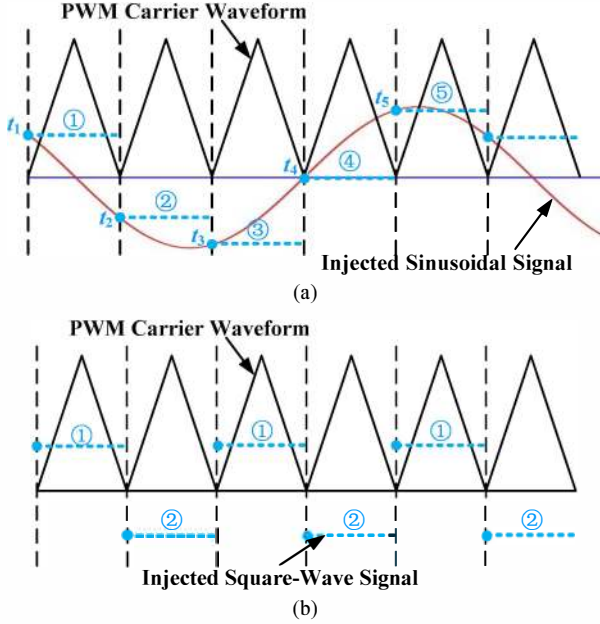

PWM Carrier Waveform

Injected Sinusoidal Signal

(a)

PWM Carrier Waveform

Injected Square-Wave Signal

(b)

Fig. 4.   Relationships between a PWM carrier signal and (a) an injected sinusoidal signal; (b) an injected square-wave signal.

B.   Square-Wave Signal Injection

As described by (8) and (9), in the proposed method, to extract the rotor position information, only the envelopes of $i_{\alpha\beta,h}$ are needed. Since the envelopes are mainly constituted by the extremes of the current waveforms, which correspond to the maximum and minimum of the injected voltage signal, i.e., values at t_5 and t_3; while other values of the injected voltage signal, e.g., the values at t_1, t_2 and t_4, are not critical. To increase the bandwidth of the sensorless speed controller and make the proposed method more effective, this paper proposes to inject a square-wave signal, as shown in Fig. 4(b). The highest frequency of the injected square-wave signal is at least more than twice the frequency of the sinusoidal signal. If the sampling frequency and control loop frequency can be doubled, i.e., the reference values of the voltages v_d and v_q can be updated twice per PWM cycle, the highest frequency of injected square-wave signal is equal to the PWM frequency.

A square-wave voltage vector, as illustrated in Fig. 4(b) and expressed as

$$v_{\gamma\delta,h} = \begin{bmatrix} v_{\gamma,h} \\ v_{\delta,h} \end{bmatrix} = V_h \begin{bmatrix} (-1)^n \\ 0 \end{bmatrix} \quad (10)$$

can be injected into γ and δ axes, where n is the index of the PWM cycles. When n is odd,

$$\begin{bmatrix} v_{d,h} \\ v_{q,h} \end{bmatrix} = V_h \begin{bmatrix} -\cos(\Delta\theta) \\ \sin(\Delta\theta) \end{bmatrix} \text{ and } \begin{bmatrix} i_{d,h} \\ i_{q,h} \end{bmatrix} = V_h \begin{bmatrix} -\cos(\Delta\theta)/Z_{d,h} \\ \sin(\Delta\theta)/Z_{q,h} \end{bmatrix} (11)$$

Then,

$$\begin{bmatrix} i_{\alpha,h} \\ i_{\beta,h} \end{bmatrix} = V_h \begin{bmatrix} -\dfrac{\cos(\Delta\theta)}{Z_{d,h}}\cos(\theta_{re}) - \dfrac{\sin(\Delta\theta)}{Z_{q,h}}\sin(\theta_{re}) \\[2mm] -\dfrac{\cos(\Delta\theta)}{Z_{d,h}}\sin(\theta_{re}) + \dfrac{\sin(\Delta\theta)}{Z_{q,h}}\cos(\theta_{re}) \end{bmatrix} \quad (12)$$

If $Z_{d,h} \approx Z_{q,h} \approx Z_{s,h}$, (12) can be further simplified as:

$$\begin{bmatrix} i_{\alpha,h} \\ i_{\beta,h} \end{bmatrix} = \frac{V_h}{Z_{s,h}} \begin{bmatrix} -\cos(\theta_{re} - \Delta\theta) \\ \sin(\theta_{re} - \Delta\theta) \end{bmatrix} = \frac{V_h}{Z_{s,h}} \begin{bmatrix} -\cos(\hat{\theta}_{re}) \\ \sin(\hat{\theta}_{re}) \end{bmatrix} \quad (13)$$

When n is even,

$$\begin{bmatrix} v_{d,h} \\ v_{q,h} \end{bmatrix} = V_h \begin{bmatrix} \cos(\Delta\theta) \\ -\sin(\Delta\theta) \end{bmatrix} \text{ and } \begin{bmatrix} i_{d,h} \\ i_{q,h} \end{bmatrix} = V_h \begin{bmatrix} \cos(\Delta\theta)/Z_{d,h} \\ -\sin(\Delta\theta)/Z_{q,h} \end{bmatrix} (14)$$

Then,

$$\begin{bmatrix} i_{\alpha,h} \\ i_{\beta,h} \end{bmatrix} = V_h \begin{bmatrix} \dfrac{\cos(\Delta\theta)}{Z_{d,h}}\cos(\theta_{re}) + \dfrac{\sin(\Delta\theta)}{Z_{q,h}}\sin(\theta_{re}) \\[2mm] -\dfrac{\cos(\Delta\theta)}{Z_{d,h}}\sin(\theta_{re}) - \dfrac{\sin(\Delta\theta)}{Z_{q,h}}\cos(\theta_{re}) \end{bmatrix} \quad (15)$$

If $Z_{d,h} \approx Z_{q,h} \approx Z_{s,h}$, (15) can be further simplified as:

$$\begin{bmatrix} i_{\alpha,h} \\ i_{\beta,h} \end{bmatrix} = \frac{V_h}{Z_{s,h}} \begin{bmatrix} \cos(\theta_{re} - \Delta\theta) \\ -\sin(\theta_{re} - \Delta\theta) \end{bmatrix} = -\frac{V_h}{Z_{s,h}} \begin{bmatrix} -\cos(\hat{\theta}_{re}) \\ \sin(\hat{\theta}_{re}) \end{bmatrix} \quad (16)$$

According to (13) and (16), the final expression for the $i_{\alpha\beta,h}$ can be expressed as:

$$\begin{bmatrix} i_{\alpha,h} \\ i_{\beta,h} \end{bmatrix} = \frac{V_h}{Z_{s,h}} \begin{bmatrix} \cos(\theta_{re} - \Delta\theta) \\ -\sin(\theta_{re} - \Delta\theta) \end{bmatrix} = (-1)^n \frac{V_h}{Z_{s,h}} \begin{bmatrix} -\cos(\hat{\theta}_{re}) \\ \sin(\hat{\theta}_{re}) \end{bmatrix} \quad (17)$$

Then by detecting the envelopes of the current components in (17), the estimated rotor position can be extracted as follows:

$$\begin{cases} \tilde{i}_{\alpha,h} = -\dfrac{V_h}{Z_{s,h}}\cos(\hat{\theta}_{re}) \\[3mm] \tilde{i}_{\beta,h} = +\dfrac{V_h}{Z_{s,h}}\sin(\hat{\theta}_{re}) \end{cases} \text{ and } \hat{\theta}_{re} = -\tan^{-1}\left(\dfrac{\tilde{i}_{\beta,h}}{\tilde{i}_{\alpha,h}} \right) \quad (18)$$

where $\tilde{i}_{\alpha,h}$ and $\tilde{i}_{\beta,h}$ are the envelopes of $i_{\alpha,h}$ and $i_{\alpha,h}$, respectively.

IV.   The Overall Sensorless SPMSM Control System

Fig. 5 shows the overall block diagram of the sensorless control system for an SPMSM operating in the low-speed region. The proposed square-wave signal injection-based position estimator is integrated with a standard space vector controller. The control system consists a speed proportional-integral (PI) regulator, which generates the command torque based on the speed tracking error. The base torque is the maximum torque at each speed point, which can be obtained

from a two-dimensional lookup table. Since the variation of the DC bus voltage will also affect the current regulation, a voltage/speed ratio is used in the controller. The current commands are generated by two lookup tables based on the torque percentage and voltage/speed ratio. In addition, current PI regulators with feedforward voltage compensation, and other conventional modules for space vector control, such as a 3-phase inverter, space-vector PWM (SVPWM) module, Park transformation, are also modeled.

To estimate the rotor position in the low-speed region, a

high-frequency square-wave voltage signal described by (10) is added to the fundamental d-axis reference voltage generated by the current regulator. The resultant phase currents, i_a, i_b and i_c, will contain high-frequency components. Low-pass filters (LPFs) are used to filter out the high-frequency components; the resultant fundamental current components are sent back to the current regulators. Therefore, the control performance will not be affected by the injected signals.

In the position estimator, the currents $i_{\alpha\beta}$ are obtained from the unfiltered i_a, i_b and i_c. The band-pass filter (BPF) is used
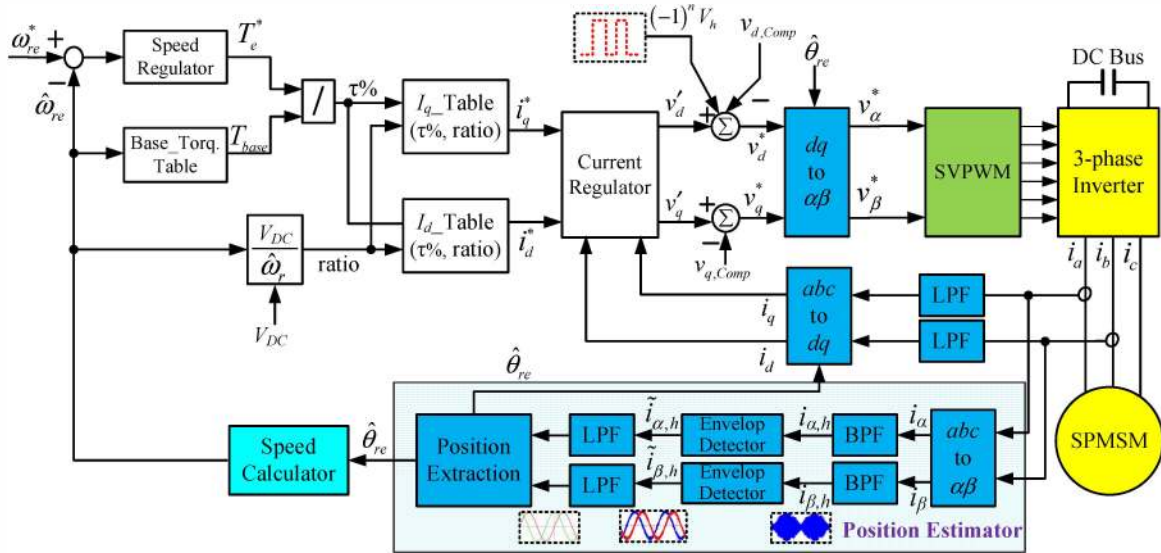

Fig. 5.   The overall block diagram of the proposed SPMSM sensorless drive system for low-speed operation.
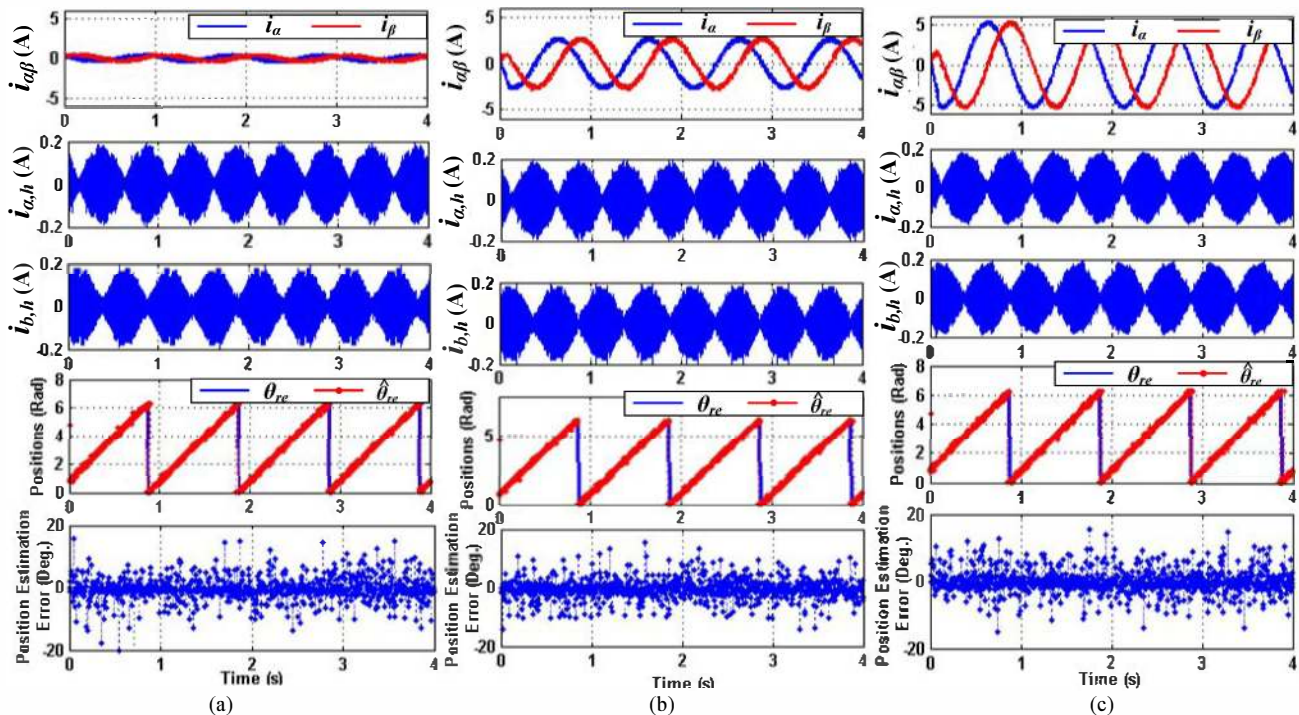

Fig. 6.   Simulation results of the sensorless SPMSM drive system, when the fundamental eletcrical frequency of currents is 1 Hz: (a) zero torque; (b) 50% of rated torque; and (c) rated torque.

to extract the current components $i_{\alpha\beta,h}$ at a certain frequency. The envelope detector is then used to obtain the envelopes of $i_{\alpha\beta,h}$, which contain the information of the rotor position. The envelope detector can be designed by using a squaring and low-pass filtering scheme or the Hilbert transform [16]. In practical applications, a suitable zero-order hold is also an alternative for envelope detection [16]. Since harmonics are present in the envelopes, LPFs are utilized to extract the desired signals, which are then used for position calculation.

V.　SIMULATION RESULTS

The key parameters of the SPMSM used in the simulation are: R_s = 3.1 Ω, L_s = 58.1 mH, λ_m = 0.452 Vs/rad, rated power = 3 hp, base speed = 1250 RPM, rated torque = 12 N·m, and the number of pole pairs is 4. The simulation results of the SPMSM sensorless drive system under different torque conditions, when the fundamental electrical frequency of $i_{\alpha\beta}$ (ω_e) is 1 Hz, are shown in Fig. 6. In the simulation, the PWM switching frequency and current sampling frequency are 3 kHz. The frequency of the injected square-wave voltage signal is 1 kHz. Fig. 6 shows the responses of $i_{\alpha\beta}$, $i_{\alpha,h}$, and $i_{\beta,h}$, the estimated and measured positions, and the position estimation error for each torque condition. At 1 Hz and under different torque conditions, the position estimation error always oscillates around $0°$ and no phase shift is observed. The position estimation error is limited within an acceptable range and the torque (or current) can be well regulated by the sensorless drive system.

To verify a wide speed control bandwidth of the proposed position estimation scheme and sensorless drive system, results for speed control from ω_e = 1 Hz (15 RPM) to ω_e = 53.3 Hz (800 RPM) are shown in Figs. 7 and 8. To guarantee good speed tracking performance in the medium-speed range (5%-100% of the base speed) as well, the PWM switching frequency and the injected signal frequency are increased to 4 kHz and 2 kHz, respectively. As shown in Fig. 7, in the speed control mode, the actual machine speed tracks the reference speed well from 15 RPM to 800 RPM. Fig. 8 depicts the profiles of $i_{\alpha,h}$ and $i_{\beta,h}$ and their position dependent envelopes at 800 RPM. These results indicate that the proposed method is effective up to 800 RPM, which is 66% of the rate speed. At this speed, the back EMF-based position estimation scheme [4] is also effective. Therefore, it is convenient to transit from the proposed method used in the low-speed range to the back EMF-based method used in the medium- and high-speed range.

VI.　EXPERIMENTAL RESULTS

A.　Experimental System Description

An experimental test stand is designed to further verify the effectiveness of the position estimation scheme and overall sensorless drive system. In the test stand, two identical 2.4-kW SPMSMs are connected back to back, as shown in Fig. 9(a). Each SPMSM has its own controller and inverter/rectifier board. The test SPMSM can work as either a generator or a motor. Therefore, both sensorless speed and torque controls can be performed on the test stand.
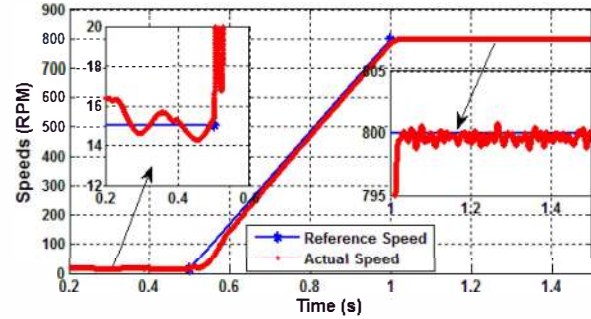

Fig. 7. Simulation result of sesnorless speed control in the low- and medium-speed range.
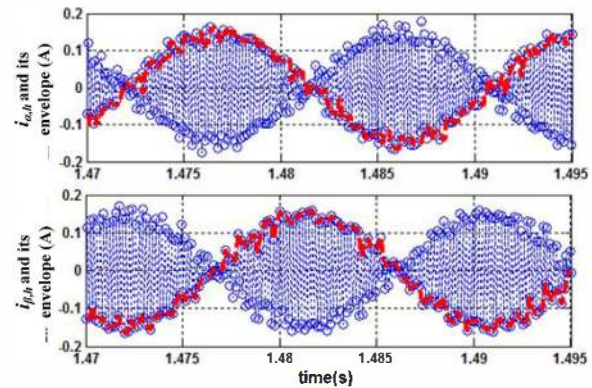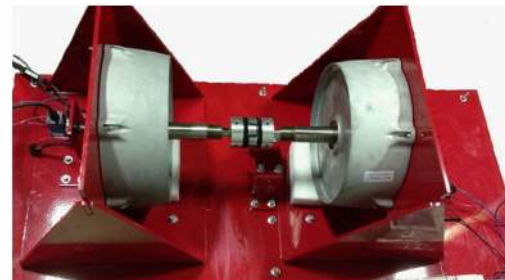

Fig. 8. Profiles of $i_{\alpha,h}$ and $i_{\beta,h}$ and their envelopes at 800 RPM (ω_e = 53.3 Hz).

(a)

(b)

Fig. 9. Test stand steup: (a) back-to-back connection of two identical SPMSMS and (b) cross section of the 42-pole test SPMSM.

The test SPMSM has 42 magnetic poles, and its cross section is shown in Fig. 9(b). Other machine parameters are listed in Table 1. In the experiments, the rotor position is measured from an absolute encoder with 8192 steps per mechanical
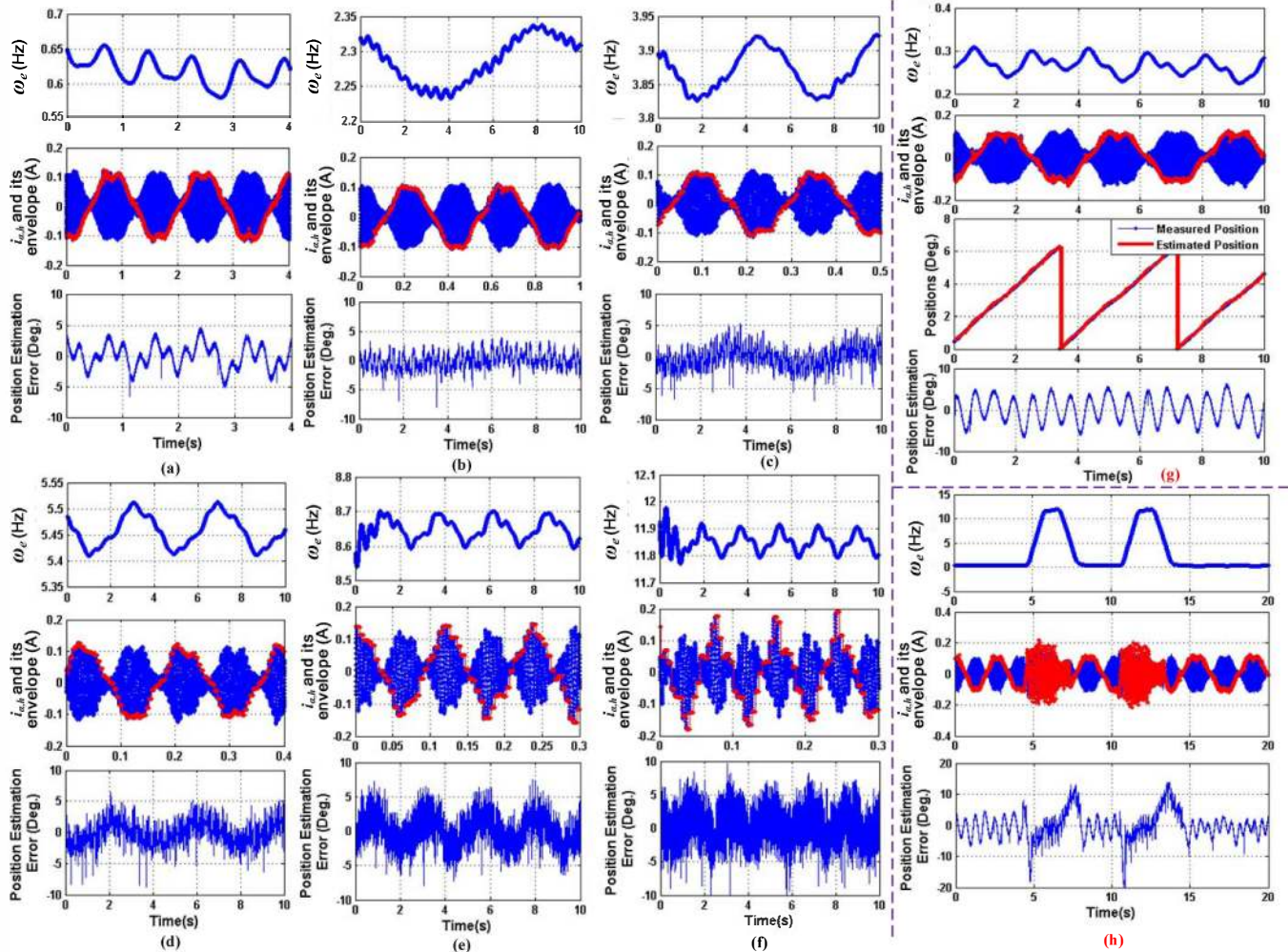
Fig. 10.   Experimental results of sensorless speed control: (a) v_q = 2.5 V and ω_e = 0.6 Hz; (b) v_q = 5 V and ω_e = 2.3 Hz; (c) v_q = 7.5 V and ω_e = 3.87 Hz; (d) v_q = 10 V and ω_e = 5.45 Hz; (e) v_q = 15 V and ω_e = 8.65 Hz; (f) v_q = 20 V and ω_e = 11.85 Hz; (g) v_q = 2 V and ω_e = 0.28 Hz; and (h) ramp speed test.

revolution for comparison purpose. The overall control algorithm is implemented in a dSPACE 1005 real-time control system with a sampling period of 100 μs. All of the experimental results are recorded using the ControlDesk interfaced with the dSPACE 1005 and a laboratory computer.

When the test SPMSM works as a motor, the shaft speed is regulated. Since the rotating speed is proportional to the value of v_q, by using different v^*_q, different rotating speeds can be achieved. At the same time, a 200 Hz square-wave voltage vector is used as v^*_d, whose magnitude is 0.5 V. The PWM switching frequency is 2 kHz. Experimental results for the sensorless speed control are shown in Fig. 10 for different speed conditions. In each case the speed is almost constant, and the profiles of the measured ω_e, $i_{\alpha,h}$ and its envelope, and the position estimation error are plotted.

In the lowest speed case shown in Fig. 10(g), ω_e is lower than 0.3 Hz. The machine shaft speed is well regulated, and the position estimation error is limited within ±6 electric degrees. The corresponding phase currents, i_a and i_b, which contain both fundamental and high-frequency components, are shown in Fig. 11. The time scale in Fig. 11 is 500 ms per division. Since the frequency of the injected signal is 200 Hz,

in the highest speed case in Fig. 10(f) where ω_e is 12 Hz, there are less than 17 (≈200/12) samples per electric revolution. With this sampling ratio, the machine shaft speed is still well regulated, and the position estimation error is limited within an acceptable range of ±10 electric degrees, which, however, is larger than other cases with higher sampling ratios. Due to the limitation of the DC-bus voltage and the cutoff frequency of the LC filter on the inverter board, the frequency of the injected signal cannot be further increased. However, as the obvious trend shown in Fig. 10, if the frequency of the injected signal can be further increased, the SPMSM can be well controlled for higher operating speed. The results for the ramp speed test are show in Fig. 10(h), where the reference speed is increased and decreased linearly between 0.3 and 12 Hz. In this circumstance, the rotor speed is also well regulated.

TABLE I
SPECIFICATION OF THE SPMSM AND SENSORLESS DRIVE SYSTEM

Nominal power	2.4 kW	Stator resistance	1.5 Ω
Number of pole-pairs	21	Base speed	300 RPM
d-axis inductance	0.87 mH	q-axis inductance	0.91 mH
Saliency ratio	2.25%	DC bus volatge	80 V

When the test SPMSM works as a generator, the output torque of the machine is regulated. The shaft speed of the test SPMSM is maintained by the other SPMSM, which works in the speed control mode. The AC power generated by the test SPMSM is converted to DC power by a three-phase IGBT converter. A DC electronic load is connected in parallel with a DC source to consume the generated electric power. The function of the DC source is to stabilize the DC-terminal voltage of the converter. Some typical experimental results of the sensorless torque control are shown in Fig. 12. The test SPMSM generates the rated torque and ω_e is maintained at 3 Hz. The result shown in Fig. 12 is consistent with the simulation result shown in Fig. 6, since no load-dependent position offset is observed. The magnitude of the position estimation error is also close to that in the no-load case.
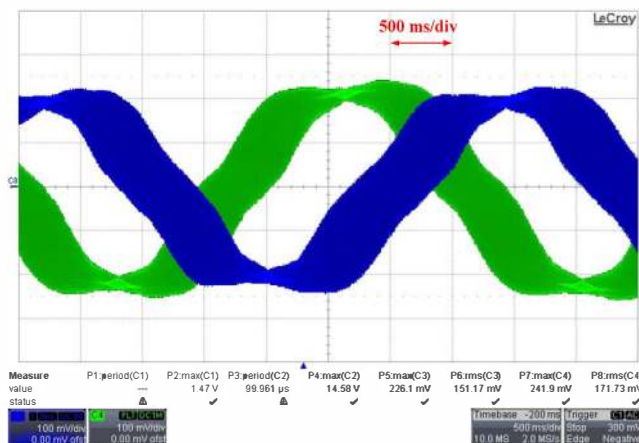

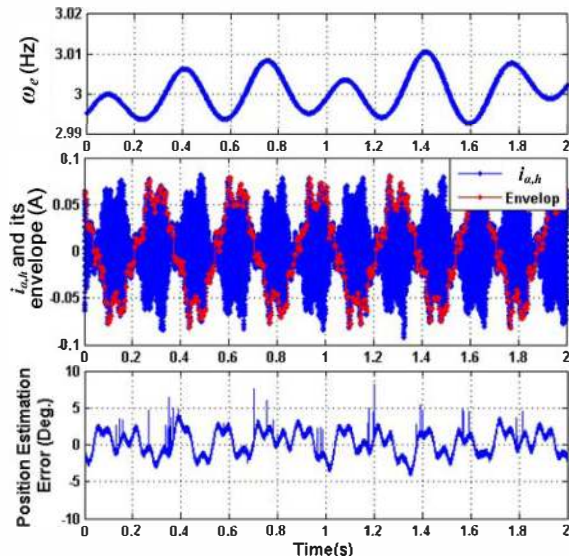Fig. 11.   Phase current (i_a and i_b) waveforms in the case of Fig. 10(g).

Fig. 12.   Experimental results of sensorless torque control, when $\omega_e = 3$ Hz and the SPMSM generates the rate torque.

VII.   CONCLUSION

A square-wave voltage injection-based rotor position estimation scheme has been proposed for SPMSMs operating in the low-speed range. In the proposed scheme, the signal is injected in the estimated rotating reference frame; the rotor position is then estimated from the envelopes of the induced current components in the stationary reference frame. The proposed method has almost no dependence on rotor spatial saliency. Therefore, it is well suited for SPMSM applications. By using the square-wave signal injection, the upper bandwidth of the speed controller can be at least twice higher than that when using the sinusoidal signal injection. The proposed position estimation scheme and sensorless control have been validated by simulation and experimental results.

REFERENCES

[1]   M. Pacas, "Sensorless drives in industrial applications," *IEEE Industrial Electronics Magazine*, vol. 5, no. 2, pp. 16-23, June 2011.

[2]   J. Holtz, "Sensorless control of induction machines—with or without signal injection?" *IEEE Trans. Ind. Electron.,* vol. 53, no. 1, pp. 7-30, Feb. 2006.

[3]   Z. Chen, M. Tomita, S. Doki, and S. Okuma, "An extended electromotive force model for sensorless control of interior permanent-magnet synchronous motors," *IEEE Trans. Ind. Electron.*, vol. 50, no. 2, pp. 288- 295, Apr. 2003.

[4]   Y. Zhao, W. Qiao, and L. Wu, "An adaptive quasi-sliding-mode rotor position observer-based sensorless control for interior permanent magnet synchronous machines," *IEEE Trans. Power Electronics*, vol. 28, no. 12, pp. 5618-5629, Dec. 2013.

[5]   I. Boldea, M. Paicu, and G. Andreescu, "Active flux concept for motion sensorless unified ac drives," *IEEE Trans. Power Electronics,* vol. 23, no. 5, pp. 2612–2618, Sep. 2008.

[6]   Y. Zhao, W. Qiao, and L. Wu, "Position extraction from a discrete sliding-mode observer for sensorless control of IPMSMs," in *Proc. IEEE Int. Symposium on Industrial Electronics,* Jun 2012, pp.725-730.

[7]   M. Corley and R. Lorenz, "Rotor position and velocity estimation for a salient-pole permanent magnet synchronous machine at standstill and high speeds," *IEEE Trans. Ind. Appl.,* vol. 34, no. 4, pp. 784-789, Jul/Aug 1998.

[8]   P. Jansen and R. Lorenz, "Transducerless field orientation concepts employing saturation-induced saliencies induction machines," *IEEE Trans. Ind. Appl.,* vol. 32, no. 6, pp. 1380-1393, Nov/Dec 1996.

[9]   Y. Yoon, S. Sul, S. Morimoto, and K. Ide, "High-bandwidth sensorless algorithm for AC Machines based on square-wave-type voltage injection," *IEEE Trans. Ind. Appl.,* vol. 47, no. 3, pp. 1361-1370, May/June 2011.

[10] J. Jang, S. Sul, J. Ha, K. Ide, and M. Sawamura, "Sensorless drive of surface-mounted permanent-magnet motor by high-frequency signal injection based on magnetic saliency," *IEEE Trans. Ind. Appl.,* vol. 39, no. 4, pp. 1031- 1039, July/Aug. 2003.

[11] S. Yang and R. Lorenz, "Surface permanent-magnet machine self-sensing at zero and low speeds using improved observer for position, velocity, and disturbance torque estimation," *IEEE Trans. Ind. Appl.,* vol. 48, no. 1, pp. 151-160, Jan./Feb. 2012.

[12] J. Lee, J. Hong, K. Nam, R. Ortega, L. Praly, and A. Astolfi, "Sensorless control of surface-mount permanent-magnet synchronous motors based on a nonlinear observer," *IEEE Trans. Power Electronics,* vol. 25, no. 2, pp. 290-297, Feb. 2010.

[13] J. Jang, J. Ha, M. Ohto, K. Ide, and S. Sul, "Analysis of permanent-magnet machine for sensorless control based on high-frequency signal injection," *IEEE Trans. Ind. Appl.,* vol. 40, no. 6, pp. 1595- 1604, Nov./Dec. 2004.

[14] P. Garcia, D. Reigosa, F. Briz, C. Blanco, and J. Guerrero, "Sensorless control of surface permanent magnet synchronous machines using the high frequency resistance," in *Proc. IEEE Energy Conversion Congress and Exposition,* Sept. 2011, pp.2709-2716.

[15] J. Hu, J. Liu, and L. Xu, "Eddy current effects on rotor position estimation and magnetic pole identification of PMSM at zero and low speeds," *IEEE Trans. Power Electron.,* vol. 23, no. 5, pp. 2565-2575, Sept. 2008.

[16] A. V. Oppenheim and R. W. Schafer, *Adaptive Discrete-Time Signal Processing*, 3rd Ed, Prentice Hall, 2009.